Maris polarization in the (p,pd) reaction

Yoshiki Chazono^{1,*}

¹ Department of Physics, Kyushu University, Fukuoka 819-0395, Japan (Dated: November 24, 2025)

Background: Proton-induced knockout reactions at intermediate energies provide a clean probe for nuclear clusters with relatively small theoretical uncertainties. The Maris polarization, which is the effective polarization of a particle inside a nucleus arising from nuclear absorption and spin-orbit coupling, has been used in proton knockout to determine the total angular momentum j of the removed protons. However, its manifestation in cluster knockout remains unexplored.

Purpose: We theoretically demonstrate that the Maris polarization can be observed via the vector analyzing power A_y of the proton-induced deuteron knockout (p, pd) reaction in imbalanced kinematics.

Method: We first compute the spin-correlation coefficient $C_{y,y}$ of p-d elastic scattering, which is an elementary process, to identify suitable kinematics for the Maris polarization. We then calculate A_y of the (p, pd) reaction at 250 MeV in forward kinematics for deuteron-cluster orbits with j = 1, 2, and 3.

Result: The large positive $C_{y,y}$ values around p-d scattering angles of $\sim 40^{\circ}$ are consistent with the experimental data. In the corresponding (p, pd) kinematics, the calculated A_y is positive for j=3 and negative for j=1, indicating effective upward and downward polarizations of the deuterons in the nucleus, respectively. The calculated A_y for j=2 lies between these and is not yet fully understood.

Conclusion: We theoretically demonstrate that the Maris polarization occurs in the (p, pd) reaction under imbalanced kinematics. This work will provide an indicator of the presence and orbital motion of deuteron clusters in nuclei, which have not yet been established. Further experimental and theoretical studies are required to improve the quantitative understanding of this effect, particularly for j=2.

I. INTRODUCTION

Although the independent-particle picture, wherein nucleons move almost independently in a nucleus, is well established, several nucleons can form clusters that behave as single entities. Nuclear clustering is a prominent manifestation of nonuniformity in nuclei and is relevant to, for example, α decay in heavy nuclei and the synthesis of elements in the universe [1]. Consequently, this topic has been extensively researched, both experimentally and theoretically.

Proton-induced knockout reactions provide a direct means to observe clusters and their motion in nuclei [2– 11]. In such reactions, a proton of several hundred MeV per nucleon collides with a nucleus and removes a constituent particle from it. Owing to the high incident energy, the disturbance of the residual system by the proton is small, and the reaction is approximately described as scattering between the proton and the particle to be removed [12–17]. This reduces the theoretical uncertainties relative to other reactions while extracting cluster information. Using this approach, the ONOKORO project has investigated the presence of light clustersdeuterons, tritons, 3 He, and α —in stable and unstable nuclei over a wide mass range [1, 11]. In addition, the proton-induced deuteron knockout (p, pd) reaction may be useful for exploring the three-nucleon force effects in the nuclear medium since the reaction can be regarded as proton-deuteron elastic scattering inside nuclei.

Knockout data provide the single-particle properties of the cluster to be removed, which are characterized by radial quantum number n, orbital angular momentum ℓ , and total angular momentum j. A topic closely related to extracting j is the Maris polarization—an effective polarization of the particle to be knocked out that arises from the strong nuclear absorption of a low-energy ejectile together with spin-orbit coupling [16, 18]. This effect, originally proposed by Jacob and Maris [19, 20], was observed in the proton-induced proton knockout (p, 2p) reaction using the strong spin correlation of the nucleon-nucleon elastic cross section at intermediate energies [21, 22]. Because of the generality of the mechanism, the Maris polarization is also expected to occur in cluster knockout reactions; however, this has rarely been discussed. Among the light clusters mentioned above, the deuteron, owing to its spin 1, is expected to exhibit the Maris polarization with characteristics different from those observed in nucleon knockout reactions. In this study, we numerically demonstrate the occurrence of the Maris polarization in the (p, pd) reaction.

The remainder of this paper is organized as follows. Section II describes the (p,pd) reaction within the distorted wave impulse approximation (DWIA) and briefly reviews the Maris polarization. The spin correlation coefficient $C_{y,y}$ of the elementary p-d process and the vector analyzing power A_y of the (p,pd) reaction are then introduced. Numerical results and discussion are presented in Sec. III. Finally, Sec. IV provides a summary and a perspective.

^{*} chazono.yoshiki.907@m.kyushu-u.ac.jp

II. THEORETICAL FRAMEWORK

We describe the (p, pd) reaction in forward kinematics within the DWIA framework. The deuteron bound to the target nucleus is assumed to be the same as that in free space. The incident proton, emitted proton, and knocked-out deuteron are labeled as particles 0, 1, and 2, respectively. The target (residual) nucleus is denoted as A (B) with mass number A (B). For particles or nuclei i (i = 0, 1, 2, A, B), the total energy, kinetic energy, and asymptotic momentum (in units of \hbar) are denoted as E_i , T_i , and K_i , respectively. Quantities with superscript L are evaluated in the laboratory (L) frame, whereas those without are evaluated in the center-of-mass (c.m.) frame of the p-A system. Although the Coulomb interaction is not explicitly shown in the formalism, it is included in the numerical calculation by a standard method. The spinorbit terms of the optical potentials are similarly treated. The z-axis is oriented along the beam direction, and we assume coplanar kinematics; that is, all momenta lie in the z-x plane.

A. (p,pd) reaction within DWIA

The DWIA transition matrix of the (p, pd) reaction is given by

$$T_{\mu_{1}\mu_{2}\mu_{0}\mu_{j}} = \sum_{\mu_{d}} \tilde{t}_{pd,\mu_{1}\mu_{2}\mu_{0}\mu_{d}}(\boldsymbol{\kappa}',\boldsymbol{\kappa})$$

$$\times \int d\boldsymbol{R} D_{\boldsymbol{K}_{1},\boldsymbol{K}_{2},\boldsymbol{K}_{0}}(\boldsymbol{R})$$

$$\times \sum_{m} (\ell m 1\mu_{d} | j\mu_{j}) \varphi_{n\ell j m}(\boldsymbol{R}), \qquad (1)$$

where $\tilde{t}_{pd,\mu_1\mu_2\mu_0\mu_d}$ is the transition amplitude of the elementary p-d process, and κ and κ' are the p-d relative momenta in the initial and final channels, respectively. μ_i and μ_d are the spin projections of particle i and the deuteron in nucleus A, respectively. The function D_{K_1,K_2,K_0} is defined as

$$D_{K_{1},K_{2},K_{0}}(\mathbf{R})$$

$$\equiv \chi_{K_{1}}^{(-)*}(\mathbf{R})\chi_{K_{2}}^{(-)*}(\mathbf{R})\chi_{K_{0}}^{(+)}(\mathbf{R})e^{-2iK_{0}\cdot\mathbf{R}}, \qquad (2)$$

where $\chi_{\mathbf{K}_i}$ denotes the distorted wave of particle i, and the superscripts (+) and (-) indicate that $\chi_{\mathbf{K}_i}$ satisfy the outgoing and incoming boundary conditions, respectively. $D_{\mathbf{K}_1,\mathbf{K}_2,\mathbf{K}_0}$ represents the suppression of the reaction at \mathbf{R} due to absorption. $\varphi_{n\ell jm}$ denotes the deuteron-cluster wave function bound to nucleus B, and $(\ell m 1\mu_d | j\mu_j)$ is a Clebsch-Gordan coefficient. m and μ_j denote the third components of ℓ and j, respectively.

Using Eq. (1), the triple-differential cross section

(TDX) of the (p, pd) reaction is expressed as

$$\frac{\mathrm{d}^{3}\sigma^{L}}{\mathrm{d}E_{1}^{L}\,\mathrm{d}\Omega_{1}^{L}\,\mathrm{d}\Omega_{2}^{L}} = F_{\mathrm{kin}}^{L} \frac{E_{1}E_{2}E_{\mathrm{B}}}{E_{1}^{L}E_{2}^{L}E_{\mathrm{B}}^{L}} \frac{(2\pi)^{4}}{\hbar v_{\alpha}^{L}} \frac{1}{2(2j+1)} \times \sum_{\mu_{1}\mu_{2}\mu_{0}\mu_{j}} \left| T_{\mu_{1}\mu_{2}\mu_{0}\mu_{j}} \right|^{2}, \tag{3}$$

where the kinematical factor $F_{\rm kin}^{\rm L}$ is defined as

$$F_{\rm kin}^{\rm L} \equiv \frac{E_1^{\rm L} K_1^{\rm L} E_2^{\rm L} K_2^{\rm L}}{(\hbar c)^4} \left[1 + \frac{E_2^{\rm L}}{E_{\rm R}^{\rm L}} - \frac{E_2^{\rm L}}{E_{\rm R}^{\rm L}} \frac{\boldsymbol{q}^{\rm L} \cdot \boldsymbol{K}_2^{\rm L}}{(K_2^{\rm L})^2} \right]^{-1}. \quad (4)$$

Here, $q^{\rm L} \equiv K_0^{\rm L} - K_1^{\rm L}$ is the momentum transfer, while $v_{\alpha}^{\rm L}$ is the relative speed between particle 0 and nucleus A

B. Maris polarization

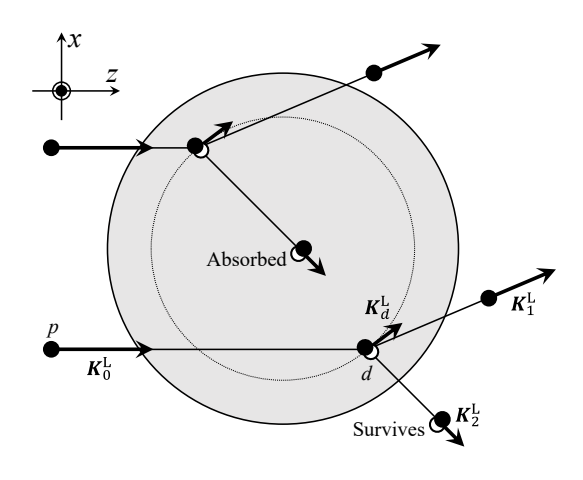


FIG. 1. Schematic of the Maris polarization.

In this section, we briefly review the Maris polarization [16, 18–22]. We consider the kinematics illustrated in Fig. 1, where $T_2^{\rm L}$ is significantly lower than $T_1^{\rm L}$. As mentioned previously, all momenta are assumed to lie on the z-x plane in this figure. The deuteron scattered at the upper side of Fig. 1 must traverse the nuclear medium to exit unlike that originated from the lower side. Because the $T_2^{\rm L} \ll T_1^{\rm L}$ condition is considered, the absorption effects on particle 2 are expected to be significantly stronger than those on particle 1. Consequently, under such imbalanced kinematics, the deuteron knocked out from the lower side of the nucleus predominantly contributes to the (p, pd) reaction. If the momentum of the internal deuteron, as estimated from momentum conservation, is $K_d^{\rm L} > 0$ (Fig. 1), it moves counterclockwise in orbit with a given ℓ in a classical picture. Considering spin-orbit coupling, three cluster orbits with $i = \ell + 1$, ℓ , and $\ell-1$ are relevant; these correspond to deuteron spins that are parallel, "orthogonal", and antiparallel to ℓ , respectively. Therefore, the combination of absorption and spin-orbit coupling generates an effective polarization of the knocked-out deuteron in nucleus A, which is called the Maris polarization.

C. Spin correlation coefficient $C_{y,y}$

In the (p,2p) reaction, the fact that the spin-triplet p-p elastic cross section considerably exceeds the spin-singlet cross section at intermediate energies is exploited to observe this effect. If the elementary p-d process exhibits a similar spin preference, the Maris polarization can be observed in the (p,pd) reaction. The spin correlation coefficient $C_{y,y}$ quantifies whether spin-parallel or spin-antiparallel scattering dominates the p-d elastic scattering.

For p-d elastic scattering, $C_{y,y}$ is defined as

$$C_{y,y} = \frac{1}{N_{pd}} \operatorname{Tr} \left[\tilde{t}_{pd} \boldsymbol{\tau}_y \boldsymbol{\sigma}_y \tilde{t}_{pd}^{\dagger} \right], \tag{5}$$

where \tilde{t}_{pd} is the 6×6 transition matrix with elements $\tilde{t}_{pd,\mu_1\mu_2\mu_0\mu_d}$. The denominator N_{pd} is calculated as

$$N_{pd} = \text{Tr}\Big[\tilde{t}_{pd}\tilde{t}_{pd}^{\dagger}\Big] = \sum_{\mu_1 \mu_2 \mu_0 \mu_d} |\tilde{t}_{pd,\mu_1 \mu_2 \mu_0 \mu_d}|^2, \quad (6)$$

which is the p-d elastic cross section without the mass factor. τ_y and σ_y are the y-components of the 6×6 deuteron and proton spin matrices, respectively. In the case of quantization along the y-axis, which is expressed by the superscript (y), these are denoted by

and

$$\boldsymbol{\sigma}_{y}^{(y)} = \begin{pmatrix} 1 & 0 & 0 & 0 & 0 & 0 \\ 0 & -1 & 0 & 0 & 0 & 0 \\ 0 & 0 & 1 & 0 & 0 & 0 \\ 0 & 0 & 0 & -1 & 0 & 0 \\ 0 & 0 & 0 & 0 & 1 & 0 \\ 0 & 0 & 0 & 0 & 0 & -1 \end{pmatrix}. \tag{8}$$

Using these, $C_{y,y}$ can be rewritten as

$$C_{y,y} = \bar{N}_{pd,++}^{(y)} + \bar{N}_{pd,--}^{(y)} - \bar{N}_{pd,+-}^{(y)} - \bar{N}_{pd,-+}^{(y)}. \tag{9}$$

The first and second terms in Eq. (9) are defined as follows:

$$\bar{N}_{pd,\pm\pm}^{(y)} = \frac{1}{N_{pd}} \sum_{\mu_1 \mu_2} \left| \tilde{t}_{pd,\mu_1 \mu_2,\pm 1/2,\pm 1}^{(y)} \right|^2.$$
 (10)

These indicate how the spin-parallel processes contribute to p-d elastic scattering, whereas the third and fourth processes, namely,

$$\bar{N}_{pd,\pm\mp}^{(y)} = \frac{1}{N_{pd}} \sum_{\mu_1 \mu_2} \left| \tilde{t}_{pd,\mu_1 \mu_2,\pm 1/2,\mp 1}^{(y)} \right|^2, \tag{11}$$

represent the contributions of the spin-antiparallel processes. Thus, $C_{y,y} > 0$ indicates the dominance of spin-parallel over spin-antiparallel processes in p-d elastic scattering, and vice versa. Kinematics with a large positive $C_{y,y}$ are therefore favorable for observing the Maris polarization.

D. Vector analyzing power A_y

The vector analyzing power A_y is suitable for measuring the Maris polarization, which is defined as

$$A_{y} = \frac{\sum_{\mu_{2}\mu_{j}} \operatorname{Tr}\left[\mathcal{T}_{\mu_{2}\mu_{j}} \sigma_{y} \mathcal{T}_{\mu_{2}\mu_{j}}^{\dagger}\right]}{\sum_{\mu_{2}\mu_{j}} \operatorname{Tr}\left[\mathcal{T}_{\mu_{2}\mu_{j}} \mathcal{T}_{\mu_{2}\mu_{j}}^{\dagger}\right]},$$
(12)

with

$$\mathcal{T}_{\mu_2\mu_j} = \begin{pmatrix} T_{1/2,\mu_2,1/2,\mu_j} & T_{1/2,\mu_2,-1/2,\mu_j} \\ T_{-1/2,\mu_2,1/2,\mu_j} & T_{-1/2,\mu_2,-1/2,\mu_j} \end{pmatrix}.$$
(13)

Here, σ_y denotes the y-component of the Pauli matrix. Equation (12) assumes that only a certain cluster orbit contributes to the (p,pd) reaction, and summations over ℓ and j are required in both the numerator and denominator when certain orbits are related to the reaction. By selecting the y-axis for quantization, Eq. (12) is reduced to

$$A_{y} = \frac{d\sigma_{+}^{(y)} - d\sigma_{-}^{(y)}}{d\sigma_{-}^{(y)} + d\sigma_{-}^{(y)}},$$
(14)

where $d\sigma_{+}^{(y)}$ ($d\sigma_{-}^{(y)}$) denotes the TDX obtained using spin-up (spin-down) incident protons. A positive (negative) A_y implies that the reaction is predominantly induced by spin-up (spin-down) particle 0. For kinematics with positive $C_{y,y}$, a positive (negative) A_y can be interpreted as the effective upward (downward) polarization of the knocked-out deuteron inside nucleus A.

III. RESULTS AND DISCUSSIONS

A. Input

We calculated the 56 Ni $(p,pd)^{54}$ Co* reaction at 250 MeV using the computer code PIKOE [17] with expansions for the (p,pd) reaction. The target nucleus is in its ground state and the residual nucleus is considered to be in the 0.94 MeV excited state. As illustrated in

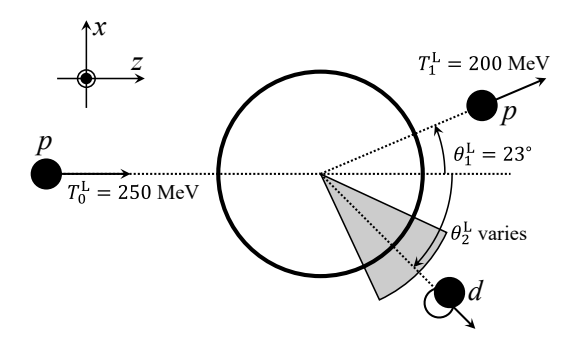


FIG. 2. Kinematics of the 56 Ni(p, pd) 54 Co* reaction.

Fig. 2, we set the kinetic energy $T_1^{\rm L}$ and the emission (polar) angle $\theta_1^{\rm L}$ to 200 MeV and 23°, respectively, and vary $\theta_2^{\rm L}$ from 25° to 65°; $T_2^{\rm L}$ remains nearly constant at ~ 30 MeV over this range. This setup corresponds to an elementary process with large positive $C_{y,y}$, as discussed in Sec. III B.

The elementary p-d amplitude $\tilde{t}_{pd,\mu_1\mu_2\mu_0\mu_d}$ is calculated from the Melbourne g-matrix interaction in free space [23]. This method has been used in Ref. [9] to describe the (p,pd) reaction, and a comparison with experimental data was performed. The calculation reasonably reproduced the data at certain energies. Details are available in Ref. [9] and the references therein.

The optical potentials with the EDAD1 parameter set [24–26] of the Dirac phenomenology were employed as distorting potentials for the p-A and p-B systems, assuming a uniformly charged sphere with the radius proposed in Ref. [27]. The wave functions of protons were multiplied by the Darwin factor, which comes from the reduction of the Dirac equation to a Shcrödinger-like one [24, 28], for the relativistic correction. For the d-B system, the global deuteron optical potential parameterized by An and Cai [29] was used. The nonlocality correction to the deuteron distorted wave was included via the Perey factor [30] with the range parameter $\beta=0.54$ fm [31].

For the deuteron cluster orbits in nucleus A, both n and ℓ were set to 2, and three j values, 1, 2, and 3 were considered. These are denoted by orbits $2D_j$. The binding potential generating $\varphi_{n\ell jm}$ is expressed as

$$V^{\mathrm{Bind}}(R) = V^{\mathrm{CE}}(R) + V^{\mathrm{SO}}(R)\boldsymbol{\ell} \cdot \boldsymbol{S} + V^{\mathrm{Coul}}(R).$$
 (15)

The central term $V^{\rm CE}$ and spin-orbit term $V^{\rm SO}$ are

$$V^{\mathrm{CE}}(R) = -V_0^{\mathrm{CE}} f(R, R^{\mathrm{CE}}, a^{\mathrm{CE}}) \tag{16}$$

and

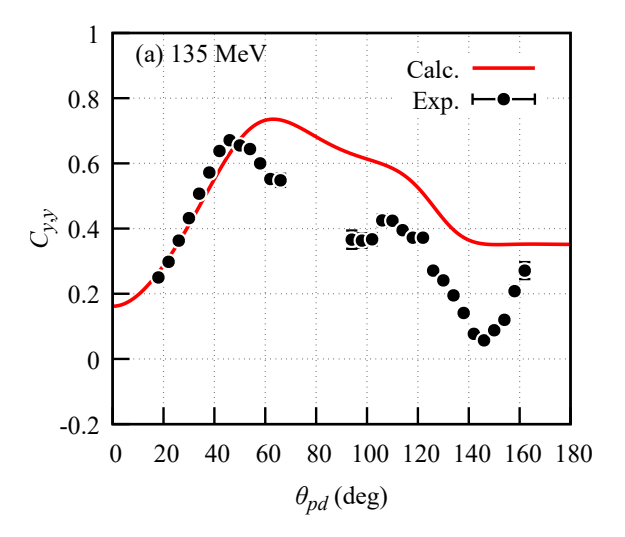
$$V^{\rm SO}(R) = -V_0^{\rm SO} \frac{2}{R} \frac{\mathrm{d}}{\mathrm{d}R} f(R, R^{\rm SO}, a^{\rm SO}),$$
 (17)

where the function f has the Woods-Saxon form:

$$f(R, R^{X}, a^{X}) = \frac{1}{1 + \exp[(R - R^{X})/a^{X}]}$$
(18)

with X = CE and SO. We set the radial parameter $R^{\rm X}=1.41\times B^{1/3}$ fm and the diffuseness to $a^{\rm X}=0.65$ fm [2]. The depth of the central term $V_0^{\rm CE}$ was adjusted to reproduce the deuteron separation energy 19.99 MeV, whereas that of the spin-orbit term $V_0^{\rm SO}$ was maintained at 10.00 MeV. The Coulomb term $V^{\rm Coul}$ uses a uniformly charged sphere with a Coulomb radius $1.41\times B^{1/3}$ fm.

B. $C_{y,y}$ of elementary process



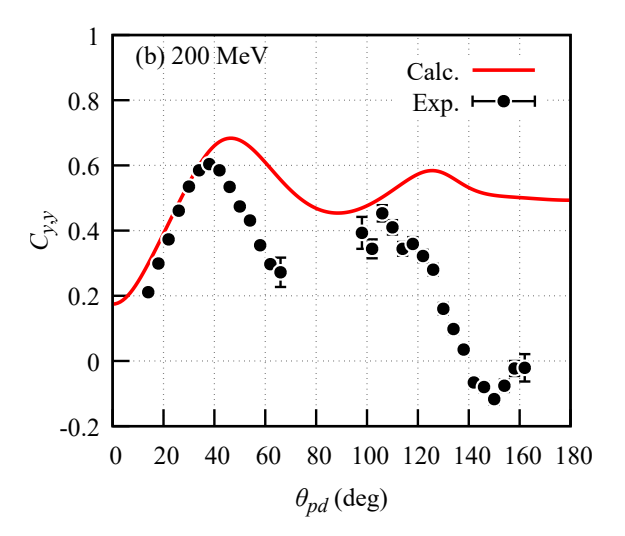


FIG. 3. Angular distribution of $C_{y,y}$ of the p-d elastic scattering at (a) 135 and (b) 200 MeV/nucleon. The scattering angle θ_{pd} is defined in the c.m. frame of the p-d system. In each panel, the numerical result (solid line) is compared with the experimental data (filled circles) [32].

Figure 3 shows $C_{y,y}$ of p-d elastic scattering as a function of the scattering angle θ_{pd} in the p-d c.m. frame. The solid lines are the results calculated at p-d scattering energies (T_{pd}) of (a) 135 and (b) 200 MeV/nucleon

using Eq. (9), which are compared with the experimental data [32] represented by filled circles. In each case, the experimental data have a large positive value around $\theta_{pd} \approx 40^{\circ}$, and its height and position indicate weak energy dependence. Although the calculations overestimate the experimental data at angles greater than (a) 50° and (b) 45°, they reproduce the data well for $\theta_{pd} \lesssim 40^{\circ}$. The setup described in Sec. III A, $\theta_2^{\rm L}=25^{\circ}, 45^{\circ}$, and 65° correspond to $\theta_{pd}\approx45^\circ$, 40°, and 35°, respectively, while the values of T_{pd} are approximately 140, 175, and 210 MeV. Unfortunately, there are limited experimental data covering a wide range of angles, so we cannot directly compare the calculation with experimental data at $T_{pd} = 175$ MeV. However, because of the weak energy dependence of $C_{y,y}$, these conditions would be favorable for observing the Maris polarization, as discussed in Sec. II C.

C. A_y of 56 Ni $(p,pd)^{54}$ Co reaction

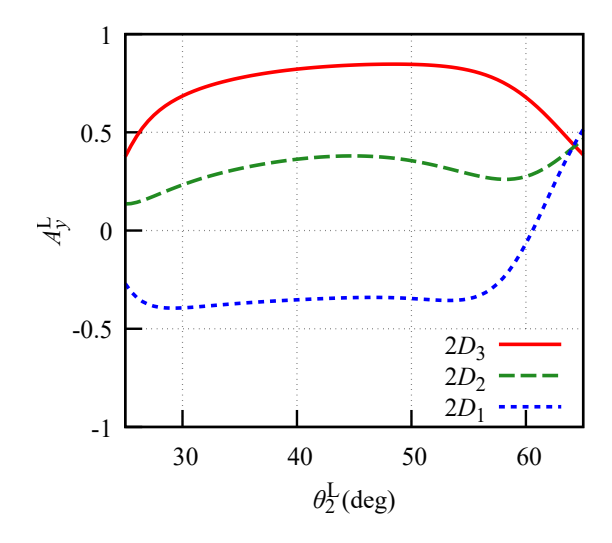


FIG. 4. A_y of the 56 Ni $(p, pd)^{54}$ Co* reaction at 250 MeV as a function of $\theta_2^{\rm L}$. The solid, dashed, and dotted lines represent the calculated results in which the deuterons to be knocked out move in orbits $2D_3$, $2D_2$, and $2D_1$, respectively.

Figure 4 shows the $\theta_2^{\rm L}$ dependence of A_y of the $^{56}{\rm Ni}(p,pd)^{54}{\rm Co}^*$ reaction at 250 MeV. The solid, dashed, and dotted lines correspond to the numerical results of deuterons to be knocked out from orbits $2D_3$, $2D_2$, and $2D_1$, respectively. The solid and dotted lines have opposite signs over almost the entire angular range, and the dashed line lies between them. As the solid (dotted) line is positive (negative), the deuteron in orbit $2D_3$ ($2D_1$) is preferentially knocked out by a spin-up (spin-down) incident proton. According to momentum conservation, the internal deuteron in nucleus A moves to the right, as shown in Fig. 1 ($K_d^{\rm L}>0$) in the considered kinematics , which corresponds to anticlockwise motion. Therefore,

the deuterons in orbits $2D_3$ and $2D_1$ are effectively polarized upward and downward, respectively, which is consistent with the mechanism explained in Sec. II B, and Fig. 4 indicates that the Maris polarization can be observed in (p,pd) under imbalanced kinematics. The dashed line, a characteristic feature of (p,pd) reactions, lies between the other two; however, the conventional Maris polarization mechanism cannot account for this behavior. Further experimental and theoretical studies are required to (i) evaluate the validity of the present calculations by comparing experimental data and (ii) fully understand the result of orbit $2D_2$.

IV. SUMMARY AND PERSPECTIVE

The Maris polarization, which is the effective polarization of a particle to be knocked out in a nucleus owing to nuclear absorption and spin-orbit coupling, has been investigated for the (p, pd) reaction within the DWIA framework. Because the deuteron has a spin 1, three j values are possible for the deuteron-cluster orbits in a target nucleus A with a given ℓ . In the present work, A_{ν} of 56 Ni $(p, pd)^{54}$ Co* at 250 MeV was calculated assuming that deuterons were knocked out from orbits $2D_1$, $2D_2$, and $2D_3$, corresponding to j = 1, 2, and 3 with $\ell = 2,$ respectively. The obtained A_y values for orbits $2D_1$ and $2D_3$ have opposite signs in the kinematics considered, which is similar to the result observed in the (p, 2p) reactions and indicates that the deuterons on these orbits in A are effectively polarized. This theoretically demonstrates the realization of the Maris polarization in the (p,pd) reaction. The results of this study will help to determine the single-particle nature of deuterons in nuclei.

In the case of deuterons knocked out from orbit $2D_2$, the calculated A_{y} is between those of orbits $2D_{1}$ and $2D_3$, which cannot be fully interpreted based on the existing mechanism of the Maris polarization, and requires further experimental and theoretical research. In addition, because deuterons are fragile particles with a binding energy of only 2.22 MeV, deuteron breakup in the elementary process and transitions induced by finalstate interactions with the residual nucleus B can affect (p, pd) observables [9], including A_y . In-medium effects, which will cause differences between the deuterons inside the nucleus and in free space, should also be considered. Since these effects were not included in the present calculations, a theoretical model beyond DWIA would be necessary for comparing calculations with experimental data.

ACKNOWLEDGMENTS

The author thanks T. Uesaka, K. Ogata, K. Yoshida, and S. Ogawa for fruitful discussions. This work was supported in part by Grants-in-Aid for Scientific Research from JSPS (Grant Nos. JP21H00125 and JP25K17393)

and JST ERATO Grant No. JPMJER2304. Numerical calculations were performed using the computer facilities

at the Research Center for Nuclear Physics, Osaka University.

- T. Uesaka and N. Itagaki, Nuclear clustering—manifestations of non-uniformity in nuclei, Phil. Trans. R. Soc. A 382, 20230123 (2024).
- [2] C. Samanta, N. S. Chant, P. G. Roos, A. Nadasen, and A. A. Cowley, Discrepancy between proton- and alphainduced cluster knockout reactions on ¹⁶O, Phys. Rev. C 26, 1379 (1982).
- [3] K. Yoshida, K. Minomo, and K. Ogata, Investigating α clustering on the surface of ¹²⁰Sn via the $(p, p\alpha)$ reaction, and the validity of the factorization approximation, Phys. Rev. C **94**, 044604 (2016).
- [4] K. Yoshida, K. Ogata, and Y. Kanada-En'yo, Investigation of α clustering with knockout reactions, Phys. Rev. C 98, 024614 (2018).
- [5] K. Yoshida, Y. Chiba, M. Kimura, Y. Taniguchi, Y. Kanada-En'yo, and K. Ogata, Quantitative description of the 20 Ne $(p,p\alpha)^{16}$ O reaction as a means of probing the surface α amplitude, Phys. Rev. C **100**, 044601 (2019).
- [6] J. Tanaka, Z. Yang, S. Typel, S. Adachi, S. Bai, P. v. Beek, D. Beaumel, Y. Fujikawa, J. Han, S. Heil, S. Huang, A. Inoue, Y. Jiang, M. Knösel, N. Kobayashi, Y. Kubota, W. Liu, J. Lou, Y. Maeda, Y. Matsuda, K. Miki, S. Nakamura, K. Ogata, V. Panin, H. Scheit, F. Schindler, P. Schrock, D. Symochko, A. Tamii, T. Uesaka, V. Wagner, K. Yoshida, J. Zenihiro, and T. Aumann, Formation of α clusters in dilute neutron-rich matter, Science 371, 260 (2021).
- [7] K. Yoshida and J. Tanaka, α knockout reaction as a new probe for α formation in α -decay nuclei, Phys. Rev. C 106, 014621 (2022).
- [8] Y. Chazono, K. Yoshida, K. Yoshida, and K. Ogata, Proton-induced deuteron knockout reaction as a probe of an isoscalar proton-neutron pair in nuclei, Phys. Rev. C 103, 024609 (2021).
- [9] Y. Chazono, K. Yoshida, and K. Ogata, Importance of deuteron breakup in the deuteron knockout reaction, Phys. Rev. C 106, 064613 (2022).
- [10] T. Edagawa, K. Yoshida, Y. Chazono, and K. Ogata, Effective polarization in proton-induced α knockout reactions, Phys. Rev. C **107**, 054603 (2023).
- [11] T. Uesaka, On the kinematics of (p, pX) knockout reactions in normal and inverse kinematics, Prog. Theor. Exp. Phys. **2024**, 083D01 (2024).
- [12] G. Jacob and Th. A. J. Maris, Quasi-free scattering and nuclear structure, Rev. Mod. Phys. 38, 121 (1966).
- [13] G. Jacob and Th. A. J. Maris, Quasi-free scattering and nuclear structure. II., Rev. Mod. Phys. 45, 6 (1973).
- [14] N. S. Chant and P. G. Roos, Distorted-wave impulseapproximation calculations for quasifree cluster knockout reactions, Phys. Rev. C 15, 57 (1977).
- [15] N. S. Chant and P. G. Roos, Spin orbit effects in quasifree knockout reactions, Phys. Rev. C 27, 1060 (1983).
- [16] T. Wakasa, K. Ogata, and T. Noro, Proton-induced knockout reactions with polarized and unpolarized

- beams, Prog. Part. Nucl. Phys. 96, 32 (2017).
- [17] K. Ogata, K. Yoshida, and Y. Chazono, PIKOE: A computer program for distorted-wave impulse approximation calculation for proton induced nucleon knockout reactions, Comp. Phys. Comm. 297, 109058 (2024).
- [18] Shubhchintak, C. A. Bertulani, and T. Aumann, Maris polarization in neutron-rich nuclei, Phys. Lett. B 778, 30 (2018).
- [19] G. Jacob, Th. A. J. Maris, C. Schneider, and M. R. Teodoro, Probing the spin-orbit coupling of nuclear protons, Phys. Lett. B 45, 181 (1973).
- [20] G. Jacob, Th. A. J. Maris, C. Schneider, and M. Teodoro, Quasi-free scattering with polarized protons, Nucl. Phys. A 257, 517 (1976).
- [21] P. Kitching, C. A. Miller, W. C. Olsen, D. A. Hutcheon, W. J. McDonald, and A. W. Stetz, Quasi-free scattering of polarized protons, Nucl. Phys. A 340, 423 (1980).
- [22] P. Kitching, W. J. McDonald, T. A. J. Maris, and C. A. Z. Vasconcellos, Recent developments in quasi-free nucleonnucleon scattering, Adv. Nucl. Phys. 15, 43 (1985).
- [23] P. J. Dortmans and K. Amos, Density-dependent effective interactions, Phys. Rev. C 49, 1309 (1994).
- [24] S. Hama, B. C. Clark, E. D. Cooper, H. S. Sherif, and R. L. Mercer, Global dirac optical potentials for elastic proton scattering from heavy nuclei, Phys. Rev. C 41, 2737 (1990).
- [25] E. D. Cooper, S. Hama, B. C. Clark, and R. L. Mercer, Global dirac phenomenology for proton-nucleus elastic scattering, Phys. Rev. C 47, 297 (1993).
- [26] E. D. Cooper, S. Hama, and B. C. Clark, Global dirac optical potential from helium to lead, Phys. Rev. C 80, 034605 (2009).
- [27] A. J. Koning and J. P. Delaroche, Local and global nucleon optical models from 1 keV to 200 MeV, Nucl. Phys. A 713, 231 (2003).
- [28] L. G. Arnold, B. C. Clark, R. L. Mercer, and P. Schwandt, Dirac optical model analysis of \vec{p} - 40 Ca elastic scattering at 180 MeV and the wine-bottle-bottom shape, Phys. Rev. C 23, 1949 (1981).
- [29] H. An and C. Cai, Global deuteron optical model potential for the energy range up to 183 MeV, Phys. Rev. C 73, 054605 (2006).
- [30] F. Perey and B. Buck, A non-local potential model for the scattering of neutrons by nuclei, Nucl. Phys. 32, 353 (1962).
- [31] TWOFNR user manual.
- [32] B. v. Przewoski, H. O. Meyer, J. T. Balewski, W. W. Daehnick, J. Doskow, W. Haeberli, R. Ibald, B. Lorentz, R. E. Pollock, P. V. Pancella, F. Rathmann, T. Rinckel, S. K. Saha, B. Schwartz, P. Thörngren-Engblom, A. Wellinghausen, T. J. Whitaker, and T. Wise, Analyzing powers and spin correlation coefficients for p+d elastic scattering at 135 and 200 MeV, Phys. Rev. C 74, 064003 (2006).